

## CHAPTER 86

Experimental investigation of the wave and current motion over a longshore bar.

J. Buhr Hansen<sup>1</sup> & Ib. A. Svendsen<sup>1</sup>

### Abstract

The results presented in this paper are from a series of experiments in a wave flume modelling the onshore-offshore water motions over a bar bottom profile.

In a true 3-dimensional natural situation the flow of water over the bar varies along the coast. In the experiments the flow of water over the bar is simulated by a controlled discharge through the flume.

### 1. INTRODUCTION

On a beach with a longshore bar there will in general be a net flow of water over the bar profile caused by the incident waves. The longshore discharge in the trough behind the bar will increase along the coast in the flow direction until it is finally released as a rip current. This study concentrates on the analysis of the on shore wave and current motion over the bar with changing net flow of water into the trough behind the bar.

In Hansen and Svendsen (1984) and Svendsen (1984) the undertow caused by waves on a plane beach with no longshore current and consequently no net on shore flow of water has been investigated. A more detailed literature review may be found in these papers and in Dally & Dean (1986) and Svendsen (1986). For completeness may be added that recently the authors have come across a note by Iwata (1970) in which some of the aspects of undertow has been discussed.

The present study shall be viewed as the first step towards a description and understanding of the full 3-dimensional water motion inside the breaker line on coasts with a longshore bar. The paper concentrates on the results of laboratory experiments aiming at an experimental verification of the theoretical model presented in Svendsen & Hansen (1986) included in these proceedings of the 20th ICCE (in the following referred to as I).

The situation studied is indicated in Fig. 1. The waves are assumed to be perpendicular to the bar and the shoreline. It is so far uncertain how the net flow of water over the bar varies along the coast. In our wave flume experiments the wave and current motion in a cross section is analysed subject to changing net flow of water over the bar simulating the varying conditions along the coast.

<sup>1</sup>Institute of Hydrodynamics and Hydraulic Engineering, Technical University of Denmark, Bygning 115, DK-2800 Lyngby, Denmark

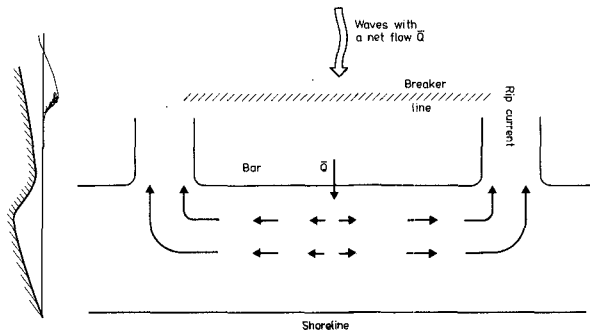


Fig. 1 The natural situation studied

2. EXPERIMENTAL SET-UP

The experiments were carried out in a 60 cm wide wave flume with a bar bottom profile, Fig. 2. The still water depth over the top of the bar is chosen to be approximately  $0.6 \cdot H$ ,  $H$  being the wave height in relatively deep water. The net flow of water is generated artificially by a closed circuit circulation of water in the flume. The water is pumped from the trough shorewards of the bar - through the wave absorber - and fed back to the flume in front of the piston type wave generator. The water is sprayed onto the surface through 60  $5 \text{ mm}^{\phi}$  holes in a 2 m long diffuser pipe placed above the water surface. The waves used through-out the experiments were generated as  $H = 12 \text{ cm}$ ,  $T = 2 \text{ s}$  using a non-sinusoidal time variation of the wave generator that yields a minimum of free harmonic disturbances. The still water depth in front of the wave generator was accurately adjusted to  $h_0 = 340 \text{ mm}$  in a situation with no waves but with the actual discharge being pumped through the flume<sup>1</sup>.

The pumped discharge,  $Q$ , is in the series of experiments performed within the range 0 to 8 l/s. (The pumped discharge will be used as indicator of the net flow in the different tests.) The mean discharge per unit length of the coast is  $\bar{Q} = 0.6 \cdot Q$ . In Table 1 the actual mean current velocities  $\bar{Q}/h$  in the different tests are given relative to

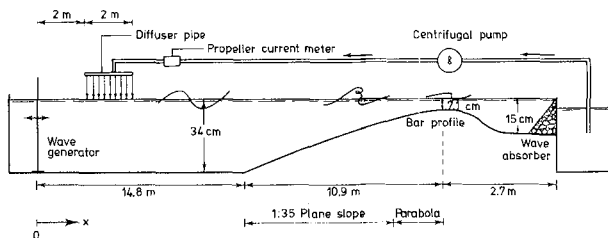


Fig. 2 Experimental set-up.

<sup>1</sup> During the tests the actual mean water depth in front of the wave-generator with both waves and current was 335 mm for the pumped discharges 0; 2.5 and 8.0 l/s but 329 mm for the discharge 5.0 l/s.

$\sqrt{gh}$  at different water depths, and relative to the measured wave particle velocity amplitude,  $1/2(u_{w,c} - u_{w,t})$ , at the bar crest.  $u_{w,c}$  and  $u_{w,t}$  are the wave particle velocities under the crest and through, respectively.

Q l/s	'h=340mm'	$\frac{\bar{Q}}{h\sqrt{gh}}$ at		$\frac{\bar{Q}}{h1/2(u_{w,c} - u_{w,t})}$
		breaking	bar crest	bar crest
0	0	0	0	0
2.5	0.0069	0.014	0.056	0.40
5	0.0141	0.030	0.128	0.85
8	0.0219	0.050	0.181	1.36

Table 1. Wave and current combinations

The chosen system for flow generation in the flume has proven to be very successful since wave recording 1 m after the diffuser pipe has given heights  $\bar{H} = 129$  mm with a standard deviation of only 2 %. There is found no significant change due to changing discharge. The recorded wave height is 8 % greater than the wave height anticipated from the wave generator motion. This is due to the fact that the wave generator motion is calculated assuming a Stokes 2. order theory, while the Stokes parameter  $UR = HL^2/h^3 \approx 36$  indicates that a higher order theory ought to be applied.

### 3. EXPERIMENTAL TECHNIQUE AND DATA ACQUISITION

For each discharge two independent sets of experiments were performed.

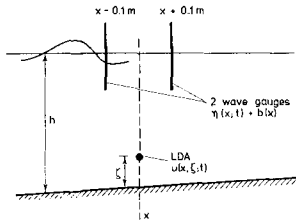
Initially a 'continuous' recording of the wave height  $H$ , the mean water surface MWS of set-up,  $b$ , and the wave celerity,  $c$ , was performed using the slowly travelling carriage technique described in Hansen and Svendsen (1979). In each of the test runs approximately 500 waves were recorded from 1 m after the diffuser pipe ( $x = 5$  m) to 0.6 m after the bar crest ( $x = 26,3$  m).

Subsequently a series of particle velocity measurements were made at selected vertical sections, and at a number of points between the bottom and the wave trough. In each of these tests simultaneous recordings were made by three wave gauges; One gauge at a fixed position 1 m in front of the diffuser pipe and two gauges 20 cm apart over the point of velocity measurement as indicated in Fig. 3. The velocities were recorded by a one component Laser Doppler Anemometer type DANTEC LDA04 with a 60 cm focussing distance which enabled the recordings to be taken in the middle of the wave flume.

The LDA analog output and the analog output from the three wave gauges were sampled by a computer based datalogging system every 15 ms, equivalent to 133 samples per wave period. A total of 30 waves were recorded in each test.

Particle velocity recordings are performed at 7 x-positions in the flume with one x-position ( $x = 18,81$  m) before and 6 after breaking, the last one over the bar crest ( $x = 25,70$  m). At each x-position the velocities are measured at 10-15 different levels,  $\zeta$ , from 5 mm above

Fig. 3 Positioning of wave gauges and LDA measuring point.



the bottom to the wave through and in some cases to the MWS. Only horizontal particle velocities are recorded.

While the wave gauges are virtually unaffected by the presence of air bubbles in the water after wave breaking, bubbles may cause drop outs in the LDA signal. As the analog signal from the LDA system may be erroneous in case of drop outs, an electronic switch operated by the LDA lock detector output is installed between the LDA analog output and the datalogging system. This gives an easily detectable value (negative overflow in the ADC) in the sampled time series in case of drop out of the LDA signal. The drop outs may then be dealt with in the subsequent data analysis.

#### 4. DATA ANALYSIS PROCEDURES

##### 4.1 LDA drop outs, correction of erroneous data

The data analysis programme constructed to deal with the LDA drop outs and eventually other erroneous data operates on a three step basis

- Step 1: The time series is scanned and all drop outs are detected. Single drop out data in otherwise valid series of data are replaced by the mean value of the two neighbour values.
- Step 2: Of the remaining drop outs groups of min. 6 consecutive data ( $\sim 0.1$  s in time) are analysed for length and periodicity of occurrence. In case of a reasonably well defined period of occurrence and a reasonably constant drop out length these data are assumed to be recorded above the actual water surface and the velocities are set to zero.
- Step 3: The remaining drop outs are replaced by the ensemble average figure calculated from the remaining data in the series. Further in this step all the time series are checked for obviously erroneous data due to neighbouring drop outs or electric noise. These are replaced by the ensemble average figures.

For the wave gauge recordings never more than 1 or 2 data within a series of 4090 are detected in step 3. For the velocity recordings well below the wave trough level a maximum of 2 % of the data are detected during the checking procedures, mainly in step 1.

When the velocity measuring point is above the wave trough level the number of erroneous data may be very high. Fig. 4 shows the first 4 periods of the processed velocity time series recorded 9 mm above trough

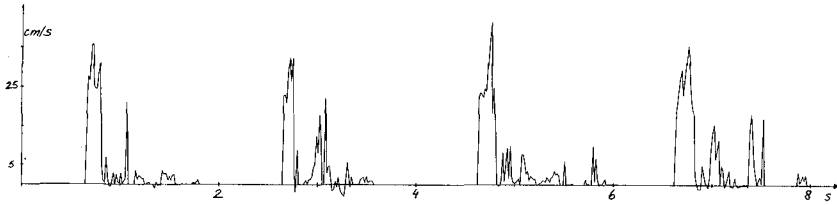


Fig. 4 Velocities recorded above the wave trough.

level at the crest of the bar where the wave height is 30 mm. In this whole series of 4090 data covering 30 wave periods 80 data are changed in step 1, 1900 set zero in step 2 and an additional 160 of the data are changed in step 3.

#### 4.2 Main results from time series

All time series are analysed over an integer number of wave periods and the following figures determined:

- 1) The zero-up-crossing mean wave period:  $T = 2.00$  s usually with a standard deviation below 0.03 s;
- 2) The mean value,  $\bar{u}$  and  $b$  for the velocity and wave gauge recordings respectively;
- 3) The mean of the maximum values ( $u_{w,c}$  and  $\eta_c$ ) and minimum values ( $u_{w,t}$  and  $\eta_t$ ) relative to the mean value;
- 4) The RMS values relative to the mean ( $RMS(u_w)$  and  $RMS(\eta)$ );
- 5) The mean 'wave heights'; and
- 6) The phase shift, or time lag  $\Delta t$ , between the signals from the two wave gauges used to determine the absolute wave celerity,  $c_a = \Delta x / \Delta t$ , with  $\Delta x = 0.2$  m, cf. Fig. 3.

#### 4.3 Separation of wave and turbulent components.

Although the waves are generated with a strictly constant wave period small and inevitable variations in the breaking may create appreciable variations in the period of each individual wave event, no matter how the period is defined. This implies difficulties in separating the turbulent part of the recorded signals from the (ordered) wave component. In fact the irregularities of both surface variation and particle motion makes it a non-trivial problem (even for strictly periodic waves) to decide what rightly is turbulence and what belongs to the wave motion (see also Svendsen, 1987).

In the present investigation we have used an ensemble average procedure to separate the turbulent part of the signal from the wave motion. This was found reasonable because the small variations in the wave periods mentioned above.

The ensemble wave component,  $\tilde{\eta}$  and  $\tilde{u}_w$  for surface elevation and velocity respectively, are then determined as the mean value of all 30 samples at the same phase of the wave. The standard deviation around each of the mean values represent the surface fluctuations,  $\eta'$ , and velocity fluctuations (turbulence),  $u'$ , respectively.

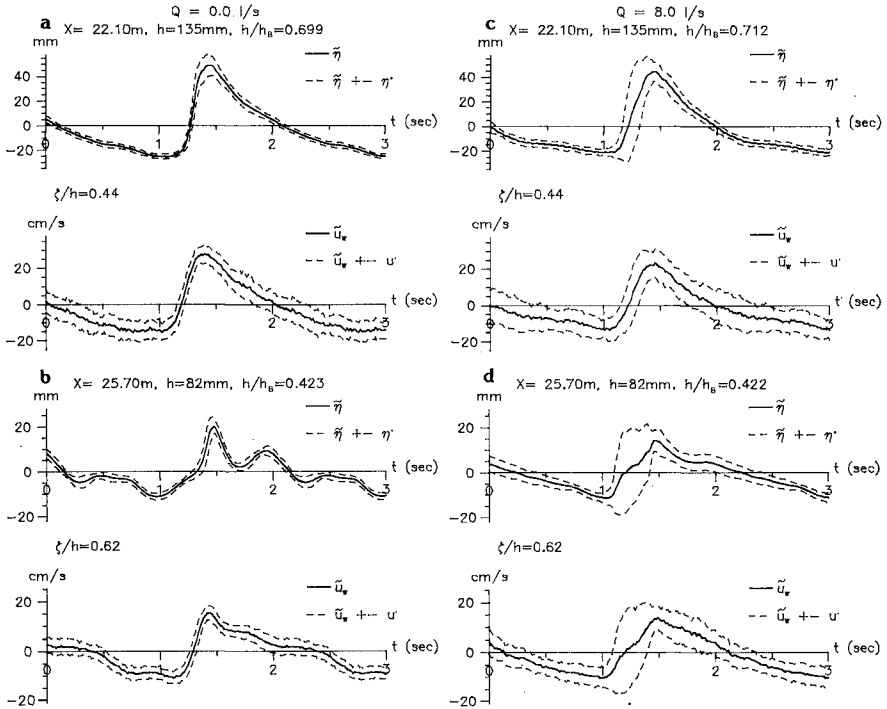


Fig. 5 Ensemble mean profiles for surface elevation,  $\tilde{\eta}$ , and wave particle velocities,  $\tilde{u}_w$ , at 2 positions for  $Q = 0$  and  $8$  l/s.

In Fig. 5 are given the ensemble mean profiles for  $\tilde{\eta}$  and  $\tilde{u}_w$  from four different tests ( $\tilde{\eta} \equiv 0$ ;  $\tilde{u}_w \equiv 0$ ). The figure 5 further shows the surface fluctuations,  $\eta'$ , and  $u'$ . In the cases a), b) and c) these are seen to be almost constant over the wave period. In Fig. 5 d), however, the level of fluctuations is considerably higher around the front of the wave than over the remaining part of the wave period. This tendency is observed only in the  $Q = 8$  l/s case and only for measuring points with  $h/h_b < 0.5$ , where  $h_b$  is the breaker depth. For these points with  $(\bar{Q}/h)/1/2(u_{w,c} - u_{w,t}) > .88$  the measured velocities are positive over the entire wave period, and the standard deviations on T is as large as  $0.2 \cdot T$ . Consequently, in that case, the  $u'$  cannot be viewed as turbulence around the wave front, but over the remaining part of the profile the  $u'$  level is virtually unaffected by the variations of the wave period.

The chosen ensemble averaging procedure will always yield signal amplitudes smaller than the mean of the individual 'heights'. In the surf zone the height of the ensemble profile is in general 0.91 times the mean of the individual heights. However, in the tests with large variations of the wave periods the ratio is as small as 0.76.

4.4 Accuracy of experimental results

From experiments using the slowly travelling carriage technique reported by Hansen & Svendsen (1979) it is established that the recorded wave heights and water level changes is very accurate. This is also the case for the measured wave celerities up to the point of breaking. In the surf zone, however, the surface fluctuations may cause widely scattered c values. As the second type of experiments performed in this study determines the wave celerity from 30 consecutive waves instead of one wave these results show much smaller scattering and will be used throughout the study.

The wave height and water level changes from the two types of experiments are in Fig. 6 seen to be in close agreement. In figure 6 the 'continuous' wave recordings are compared with the mean values from all individual waves,  $\bar{H}$  and  $b$ , recorded in the time series. The standard deviation on  $\bar{H}$  is less than 2 mm and on the set-up's less than 0.3 mm in all positions but one ( $x = 21.23$ ) which is the first measuring

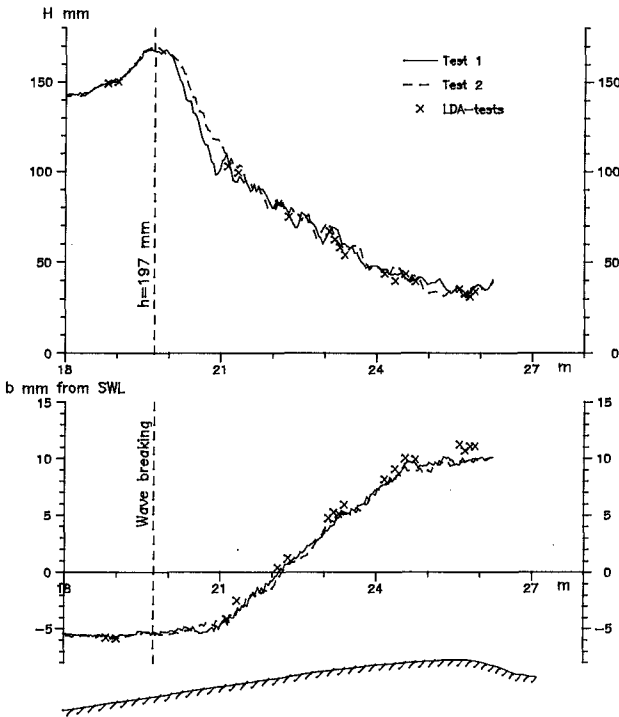


Fig. 6  
 Reproducibility of wave heights and water level changes for  $Q = 0$ . Test 1 and test 2 from 'continuous' wave recordings; LDA-tests are  $\bar{H}$  and  $b$  from time series.

position after breaking. Fig. 6 is for the  $Q = 0$  case, but the same tendency is clearly observed for other  $Q$  values.

Also the velocity measurements show a larger variation near the breaking point than elsewhere. The largest scattering obtained from repeating the same measurement several times is found at  $x = 21.23$  m. Fig. 7 shows the results for the mean velocity,  $\bar{u}$ , (undertow) from a total of 7 test series. The large variation on the mean values indicates that the 30 waves used in each test is a too small number for a proper averaging at this point. At all other points the variance is much smaller and 30 waves define the mean sufficiently accurately. The results presented in the following chapter of this paper are taken as the mean value of all tests at any particular position and height.

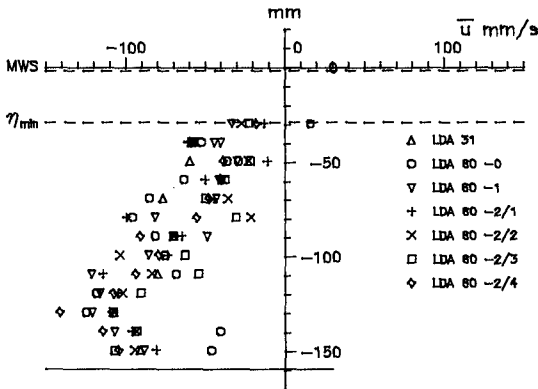


Fig. 7 Repeated measurements of undertow ( $Q = 0$ ) at  $x = 21.23$  m;  $h/h_B = 0,80$

5. DISCUSSION OF RESULTS

5.1 Surface elevations

As the waves in front of the sloping bed are seen to be virtually unaffected by the superimposed currents this may be expected also to be the case about wave breaking where  $(\bar{Q}/h)/\sqrt{gh} < 0.05$ , see Tables 1 and 2. The point of wave breaking is defined as the point with  $(H/h)_{max}$  in the 'continuous' wave recordings; the position varies from  $x = 19.34$  m for  $Q = 2.5$  l/s ( $h = 205$  mm) to  $x = 19.82$  m for  $Q = 8$  l/s ( $h = 194$  mm). When considering that small irregularities in the recorded waves may easily shift the position of  $(H/h)_{max}$  point  $\pm 20$  cm (see Fig. 6) it is reasonable to conclude that the wave breaking is not significantly influenced by the current.

From the wave data at the bar crest included in Table 2 it appears that the decay of the waves over the surf zone and the set-up,  $b_{\bar{u}}$ , are not significantly influenced by the current either. However, the  $H/h$  value at the bar crest seems to be increasing with increasing current, which might indicate that the intensity of the wave breaking is reduced with increasing flow velocity. These mechanisms are discussed more detailed in I.

All time series measurements in the surf zone are assumed to be within the inner region of the surf zone as defined in Svendsen et al (1978). This is analysed further in I.

Q l/s	At breaking (from 'continuous' wave recording)				At bar crest (from time series)			
	H <sub>B</sub> mm	Δb <sup>2)</sup> mm	h <sub>B</sub> mm	H <sub>B</sub> /h <sub>B</sub>	H̄ <sup>1)</sup> mm	Δb <sup>2)</sup> mm	h mm	H̄/h
0	170	-0,6	197	0.87	33.0	16.5	82	0.41
2.5	163	-0,8	205	0.79	37.6	17.6	83	0.45
5	162	-0,5	198	0.82	33.4	15.3	76 <sup>3)</sup>	0.44
8	156	-0,8	194	0.80	38.5	15.6	82	0.47

- 1)  $\bar{H}/H \sim 0.1$  in all tests. 2) Relative to MWS at  $h_0 = 340$  mm  
 3) See footnote p. 2

Table 2 Wave characteristics at breaking and at the bar crest

The dimensionless wave energy flux,  $B_0$ , is from Fig. 8 seen also to be unaffected by Q, but is, on the other hand, seen to vary considerably over the surf zone with a maximum at  $h/h_B \sim 0.6$  and  $H/H_B \sim 0.45$ . Fig. 8 and Fig. 9 are both included for later comparisons with the velocity measurements.

The absolute wave celerity,  $c_a$ , is significantly increasing for increasing discharge through the wave flume. As should be expected, however, the relative celerity  $c_r$  given by  $c_r = c_a - U$  (where U is the current velocity averaged over the depth) is in Fig. 10 seen to be independent of the pumped discharge.

U is determined from the results given in Fig. 11 as the mean value of  $\bar{u}$  from the bottom to MWS, where values above trough level have in most cases been obtained by extrapolation.

A possible interpretation of the results for  $c_r$  is that  $c_r = \alpha\sqrt{gh}$ . This has been used in I with an assumed constant  $\alpha$  value. The measured  $c_r$  can also be said to agree well with the bore celerity,  $c_{bore}$ , as given by

$$\frac{c_{bore}^2}{gh} = 1/2 \frac{d_t \cdot d_c}{h^3} (d_t + d_c)$$

(eq. 44 in Svendsen et al (1978), where  $d_t$  and  $d_c$  are the water depth under wave trough and crest, respectively.

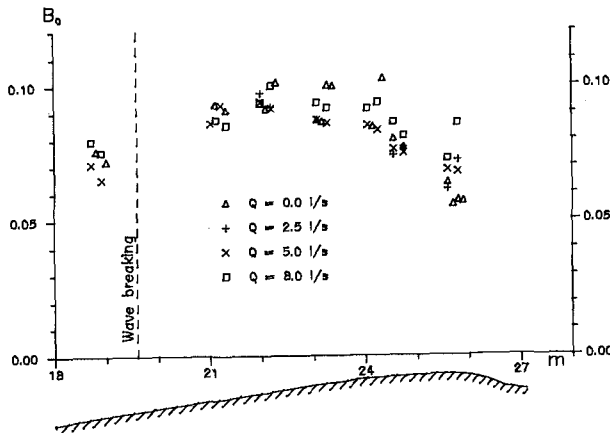


Fig. 8  $B_0 = \bar{\eta}^2/H^2$  for the ensemble mean surface profiles.

Fig. 9 Surface fluctuations  $\eta'$ .

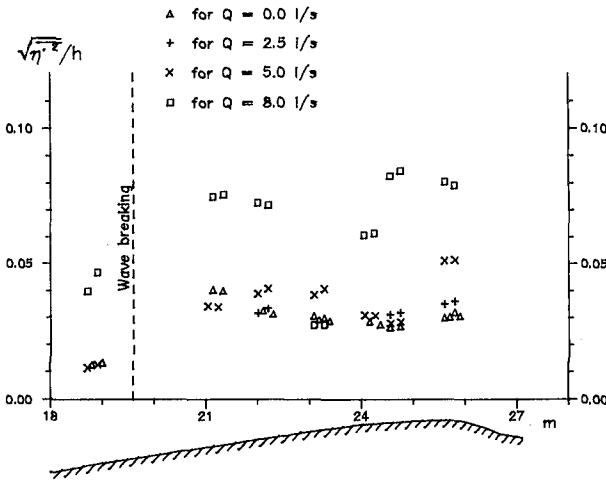
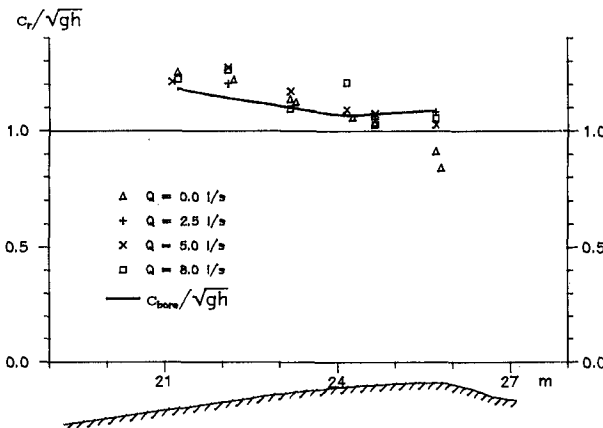


Fig. 10 Relative wave celerity



5.2 Particle velocities

Mean velocities are calculated from the time series as  $\bar{u}$  over the total number of periods. The results are compiled in Fig. 11 for all horizontal and vertical positions and for the four different discharges through the flume. The mean velocities for different discharges all show similar depth variations. Only at the two positions closest to breaking ( $x = 21.23$  m and  $22.10$  m) do the big scatter in the individual results obviously distort the general trend. As previously pointed out (see Fig. 7) the vigorous breaking and associated large variations from wave to wave in this region causes a considerable scatter in the results when averaged over -only- 30 consecutive waves.

The volume flux,  $Q_s$ , due to the waves may also be determined from

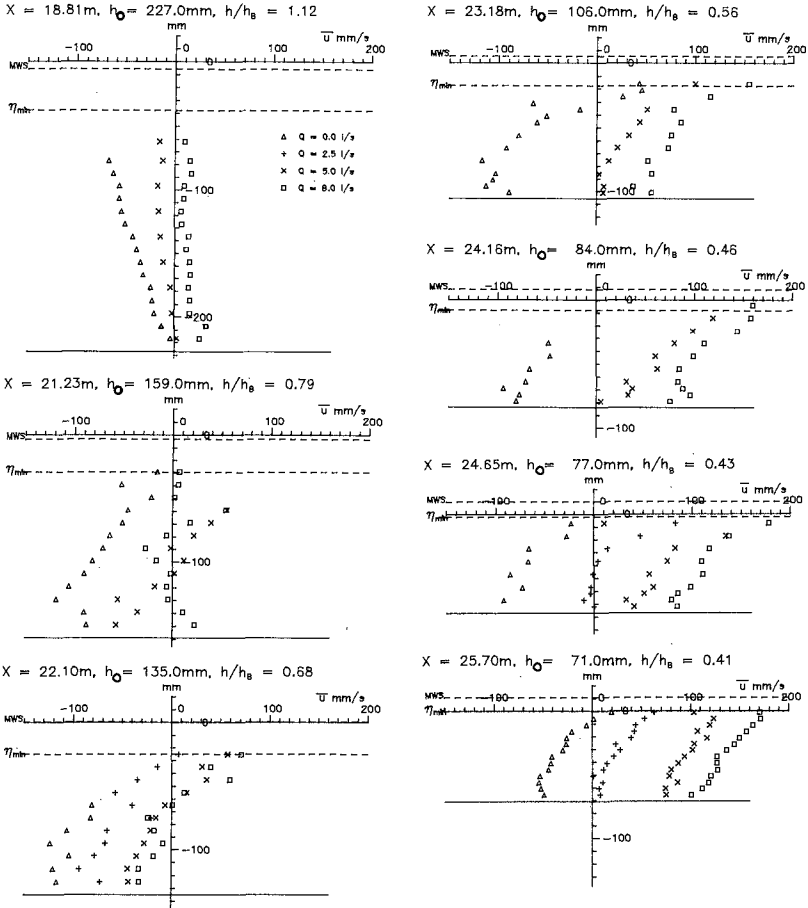


Fig. 11 Mean Eulerian velocities at 7 positions for four different  $Q$  values.

the measurements. The depth integrated, time averaged continuity equation reads  $\bar{Q} = \bar{Q}_C + \bar{Q}_S$ . Here  $\bar{Q}_C$  is the mean discharge from bottom to MWS,  $\bar{Q}_C = \bar{U} \cdot \bar{A}_S$ .  $\bar{Q}$  is known from the pumped discharge,  $\bar{Q}_S$  can be determined and the results are given in Fig. 12. They show a considerable scatter indicating how delicate these calculations are and how sensitive they are to the accuracy of the recorded  $\bar{U}$  or  $U$  values. This particularly applies to situations where  $U$  is primarily due to  $\bar{Q}$  so that  $\bar{Q}_S$  is determined as the difference between two large numbers.

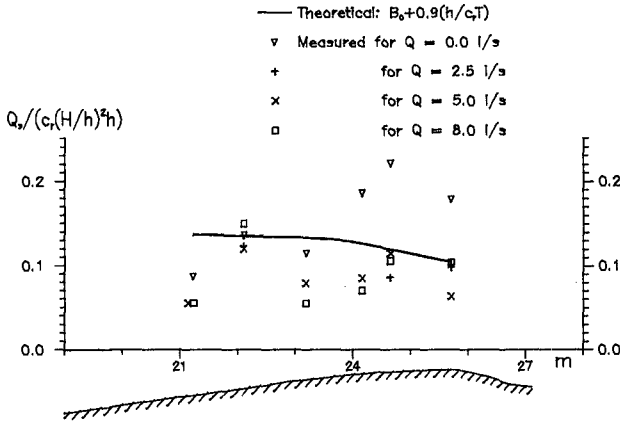


Fig. 12  
Theoretical and 'measured' mass flux  $Q_s$  due to waves.

Fig. 12 also shows the values of  $Q_s$  used in I but calculated from the measured  $c_r$  and  $H$  as given in Fig. 8 and 10. The 'theoretical'  $Q_s$  values are generally higher than the measured values.

The wave particle velocities,  $u_w$ , for  $Q = 0$  l/s and  $Q = 8$  l/s are shown in Fig. 13. For the 2.5 and 5 l/s cases the picture is exactly the same.

The relation between the surface elevations  $\eta$  and the particle velocities  $u_w$  are to the lowest order of approximation

$$u_w = \sqrt{gh} \cdot \frac{\eta}{h}$$

or, when averaged over the period

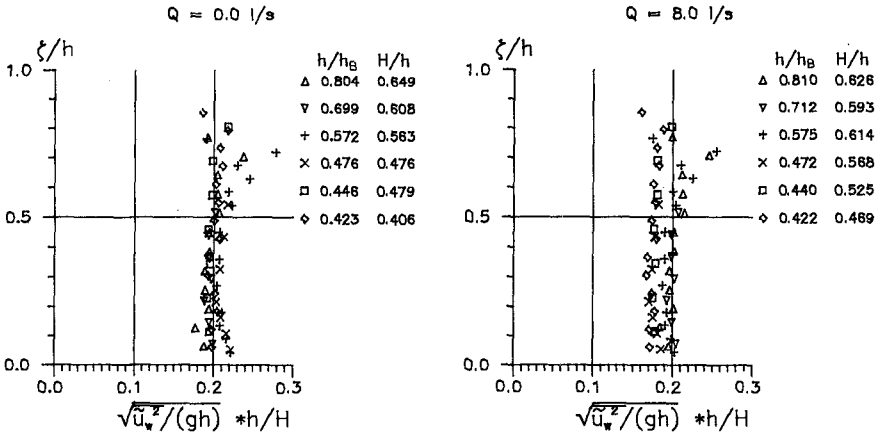


Fig. 13 Kinetic energy in ensemble mean wave particle motions.

$$\sqrt{\frac{\overline{u^2}}{gh}} \cdot \frac{h}{H} \approx \sqrt{B_0}$$

When the velocities are calculated from the surface recordings using this relation (Fig. 8 shows  $\sqrt{B_0}$  values ranging from 0.25 to 0.31) they are significantly overestimated.

The implication of this is that in the theoretical results in I  $B_0$  should only represent  $\overline{\eta^2}$ . Where  $B_0$  represents  $\overline{u^2}$  contributions a smaller value than  $B_0$  should be used. A closer analysis is left for future studies.

The velocity fluctuations (turbulence) are shown in Fig. 14 for the two cases  $Q = 0$  l/s and 8 l/s. The significant decrease in turbulence level for decreasing water depth found in the  $Q = 0$  l/s case does not appear in any of the three other current situations.

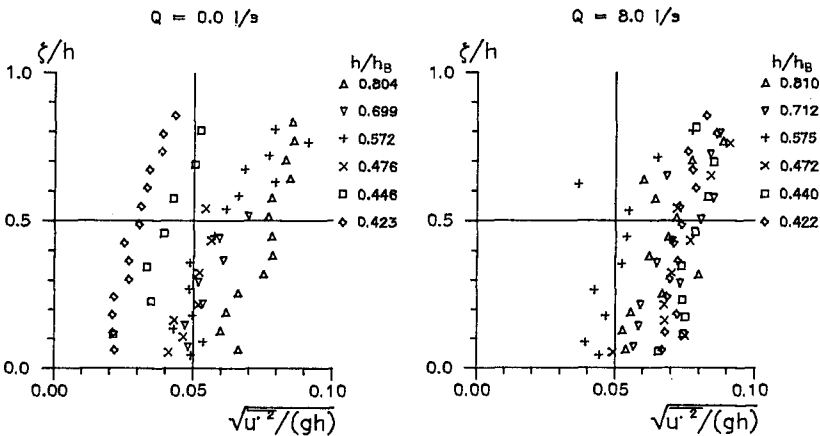


Fig. 14 Turbulent energy in recorded particle motions.

Svendsen (1987) has analysed other available data on surf zone turbulence. The total turbulent kinetic energy,  $k$ , may be estimated from  $u'$  component as

$$k = \frac{1}{2} \cdot \frac{1}{0.43} \overline{u'^2} = 1.082 \overline{u'^2}$$

(Svendsen (1987) eq. 3.1). The results given in Fig. 14 are from this seen to be in close agreement with the results of Stive & Wind's test No. 1 as analysed in Svendsen (1987). It is interesting to notice, that the level of surface fluctuations,  $\overline{\eta^2}/h^2$ , as given in Fig. 9 are of the same order of magnitude as the  $\overline{u'^2}/gh$  given in Fig. 14. The implication of this and other aspects of the turbulence will be analysed further.

The analysis of the results continues. The theoretical model given in I and the experiments reported here are used interactively to gain further insight into the problem studied.

#### 6 REFERENCES

- Dally, W.R. & R.G. Dean (1986) Discussion on: Mass flux and underflow in a surf zone, by I.A. Svendsen Coastal Engineering, 10, 289-299
- Hansen, J. Buhr & I.A. Svendsen (1979) 'Regular waves in shoaling water- Experimental data', Series paper 21, Inst. Hydrodyn. and Hydraul. Eng. (ISVA), Techn. Univ. Denmark
- Hansen, J. Buhr & I.A. Svendsen (1984) 'A theoretical and experimental study of undertow', Proc 19. International Conf. Coastal Eng., Houston, ch. 151, 2246-2262
- Iwata, N. (1970) A note on wave set-up, longshore currents and undertows, J. Oceanogr. Soc. Jap., 26, 4, 233-236
- Svendsen, I.A., P.Å. Madsen and J. Buhr Hansen (1978) 'Wave Characteristics in the Surf Zone, Proc. 16th Int. Conf. Coastal Eng., Hamburh, Vol I, chap. 29, 520-539
- Svendsen, I.A. (1984) 'Mass flux and undertow in a surf zone', Coastal Engineering 8, 4, 347-365
- Svendsen, I.A. (1986) Reply to Dally & Dean (1986) Coastal Engineering 10, 299-307
- Svendsen I.A. & J. Buhr Hansen (1986) 'The interaction of waves and currents over a longshore bar', Proc. 20. International Conf. Coastal Eng., Taipei (Denoted I in text)
- Svendsen, I.A. (1987) 'Analysis of surf zone turbulence' To be published in Journ. of Geoph. Res. (Also Danish Center for Applied Mathematics and Mechanics, Report No. 330, July 1986)